

ELASTODYNAMIC DIRECT BOUNDARY ELEMENT METHODS WITH ENHANCED NUMERICAL STABILITY PROPERTIES

B. BIRGISSON^{1,*†}, E. SIEBRITS^{2,‡} AND A. P. PEIRCE^{3,§}

¹ *Department of Civil Engineering, University of Florida, Gainesville, FL 32611-6580, U.S.A.*

² *Schlumberger Dowell, Sugar Land, TX 77478, U.S.A.*

³ *Department of Mathematics, University of British Columbia, Vancouver, Canada*

SUMMARY

Evidence of numerical instabilities in two-dimensional time domain direct boundary element methods is presented. The effects of numerical versus analytical integration of spatial integrals on stability are shown, and two new time-stepping algorithms are introduced and compared to existing formulations. The so-called new 'direct half-step' scheme and the 'epsilon' scheme are shown to improve the numerical stability of direct boundary element methods. Copyright © 1999 John Wiley & Sons, Ltd.

KEY WORDS: elastodynamics; boundary element method; time domain; numerical instability

INTRODUCTION

Over the past 30 years, a wealth of literature has been published on two-dimensional time domain elastodynamic direct boundary element methods. The reader is referred to Beskos [1] for an exhaustive summary of the literature. However, some of the more recent work includes that of Dominguez [2], Israil and Banerjee [3, 4], and Birgisson and Crouch [5]. Dominguez [2] presents a two-dimensional formulation that includes isoparametric quadratic elements with constant variation in tractions and linear variation in displacements with time. Israil and Banerjee [3, 4] summarize a two-dimensional multi-region transient elastodynamic boundary element formulation that uses isoparametric quadratic elements and constant and linear temporal variation of tractions and displacements, respectively. Birgisson and Crouch [5] introduce a general two-dimensional multi-region transient elastodynamic boundary element formulation using straight-line elements with a piecewise quadratic variation in tractions and displacements over each element, and piecewise linear variation of time within each time step. All integrations are performed analytically.

* Correspondence to: B. Birgisson, Department of Civil Engineering, University of Florida, 345 Weil Hall, P.O. Box 116580, Gainesville, FL 32611-6580, U.S.A. E-mail: bbirg@ce.ufl.edu

† Assistant Professor

‡ Senior Development Engineer

§ Professor

Unfortunately, there is growing evidence of numerical instabilities in direct elastodynamic boundary element formulations [2, 6], as well as indirect boundary element methods. Siebrits and Peirce [7] and Peirce and Siebrits [8, 9] have studied the instability problem in model problems involving the one-dimensional wave equation and in indirect boundary element methods in depth. However, the nature of instabilities in the direct boundary element method has not been studied in detail previously.

In this paper we show evidence of numerical instabilities in time domain direct elastodynamic boundary element formulations. We use the insight gained from the stability analysis of indirect elastodynamic boundary element formulations to propose time-stepping schemes for the direct boundary element method with substantially improved stability characteristics. The enhanced stability characteristics of the so-called direct half-step and epsilon schemes are clearly demonstrated by contrasting their performance with the trapezoidal scheme which is commonly used in boundary element formulations. We will only discuss two-dimensional problems here, but these new time-stepping schemes are readily applicable to three-dimensional problems.

In this paper, we first observe some typical problems with the stability of the elastodynamic time domain direct boundary element method. We then briefly summarize the boundary element equations of elastodynamics, with a description of the typical discretization procedure, followed by a discussion on the direct half-step and epsilon schemes. In particular, the stability characteristics of the epsilon scheme are reviewed and compared to the more traditional trapezoidal scheme. Finally, we contrast the performance of the epsilon and half-step schemes with the trapezoidal scheme by means of numerical examples, and make some concluding remarks.

EVIDENCE OF NUMERICAL INSTABILITIES

Relatively few papers provide clear evidence of numerical instabilities in direct boundary element methods [2, 10, 11], although some hint at the possibility [12–14]. One of the reasons for the lack of evidence of numerical instabilities in the past has been the very long computer run times and large disk storage requirements of dynamic boundary element methods. With the advent of more powerful computers the numerical instability issue has become more noticeable for two reasons. First, more time steps can be calculated. Second, more complicated geometries and loading configurations can be modeled, leading to numerical instabilities that corrupt the transient results.

The time-marching direct boundary element formulations presented by Mansur [12] and Antes [13] for two-dimensional problems illustrate increased oscillations at late times, indicating potential instabilities in some of their results. Fukui [10] notes that his numerical scheme is unstable for smaller time increments. Manolis *et al.* [14] present a three-dimensional time domain direct boundary element method, with results for less than 25 time steps. This scheme uses repeated averaging in time ‘for added accuracy’ of the method, and thus hints at the possibility of numerical problems. Tian [11] also notes numerical instabilities in his direct boundary element simulator (DBEM2), which uses piecewise linear in time and piecewise quadratic in space functional variations.

To further examine the occurrence of numerical instabilities in recently developed elastodynamic direct time domain boundary element formulations, a number of simplified problems were studied. Two recently published direct boundary element simulators were used in this

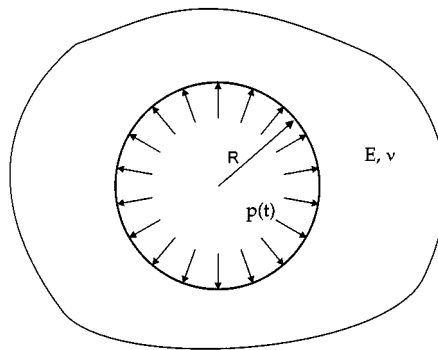


Figure 1. Suddenly loaded cylindrical cavity

study—QUADPLET [2], which uses numerical integrations for the spatial integrals, and a two-dimensional computer simulator, called DABEMs [5], in which all integrations are performed analytically. Both simulators use piecewise quadratic spatial elements, and QUADPLET uses either piecewise constant or linear temporal elements, whereas DABEMs uses piecewise linear temporal elements only.

The first problem examined, shown in Figure 1, is the response of a cylindrical cavity to a suddenly applied pressure (the so-called Selberg problem). The cavity has radius R and the applied loading is given by $p(t) = p_0 H(t)$, where $p_0/G = 10^{-3}$, and G is the shear modulus. The mass density of the surrounding domain is $\rho = 2700 \text{ kg/m}^3$, the compressional wave velocity is $c_1 = 5367 \text{ m/s}$, and the shear wave velocity is $c_2 = 3287 \text{ m/s}$. These properties correspond to a Poisson's ratio of $\nu = 0.2$, and a shear modulus of $G = 29.17 \text{ GPa}$. The time step Δt is given in terms of a dimensionless parameter

$$Q_1 = \frac{c_1 \Delta t}{a_1} \quad (1)$$

where a_1 is the element half-length. The boundary of the cavity is discretized into 16 elements and the number of time steps N_t is 3000. Figure 2 shows the calculated radial displacements plotted against the normalized time $c_1 t/R$. The results from QUADPLET [2] show signs of instability at a normalized time of $c_1 t/R = 150$, whereas the results from DABEMs [5] do not show any signs of instability during the 3000 time step run.

The second problem, shown in Figure 3, is a modified Selberg problem, in which only one-half of the cavity is loaded. The geometry, number of elements, and material constants are the same as in the Selberg problem discussed previously, except that the number of time steps is now $N_t = 2500$. As shown in Figure 4, the instability observed in QUADPLET [2] now starts at a normalized time of about $c_1 t/R = 30$. Again, the results from DABEMs [5] show no sign of instability during the 2500 time step run.

These results indicate that the use of analytical integration schemes may significantly improve the stability of elastodynamic boundary element methods. One possible explanation for the apparently superior stability properties of analytically integrated boundary element formulations is the way in which a sudden change in displacement or stress, generated when a wave front cuts partially through an element, is handled numerically. These cases require careful evaluation,

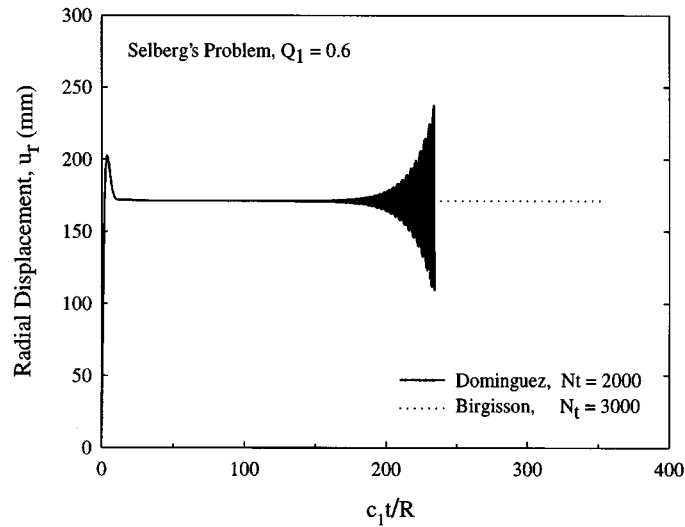


Figure 2. Radial displacement at the wall of a cylindrical cavity

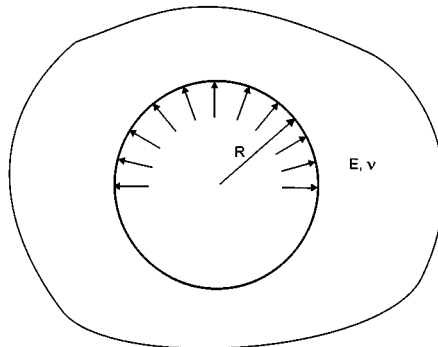


Figure 3. Partially loaded cylindrical cavity

because an influence coefficient is still generated in these cases, and if these partial influence factors are ignored, they will tend to lead to both the accumulation of round-off errors and a gradual loss of causality in the solution. In DABEMs, causality is ensured by using variable integral limits, described in detail by Siebrits and Crouch [15], so that integrations are performed only over the dynamically active parts of each element. However, in numerical integration formulations, the influence of these partial influence factors is either ignored or the element in question is divided into many small sub-elements, followed by a determination of the optimal number of Gauss points per sub-element as discussed by Israil and Banerjee [3, 4]. If an inadequate number of sub-elements or Gauss points are used, then errors due to small violations in causality and round-off will accumulate, resulting in numerical instabilities.

Another point of interest is that, in the two-dimensional fundamental solution of elastodynamics, the dynamic effects do not cease after the shear wave arrival, as is the case in three

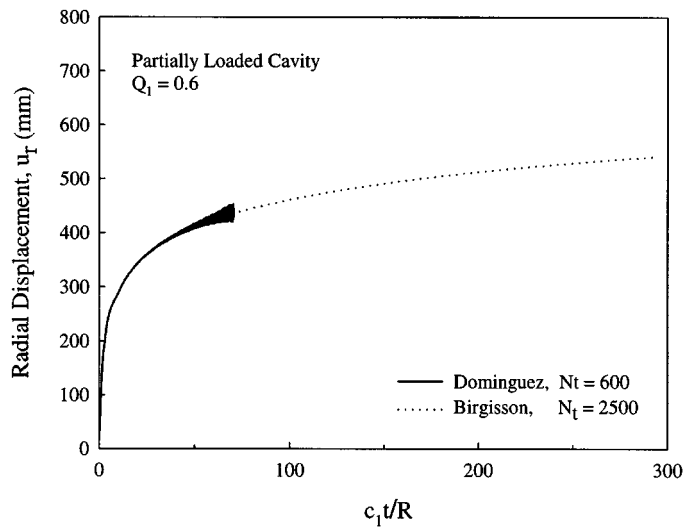


Figure 4. Radial displacement at the wall of a partially loaded cylindrical cavity

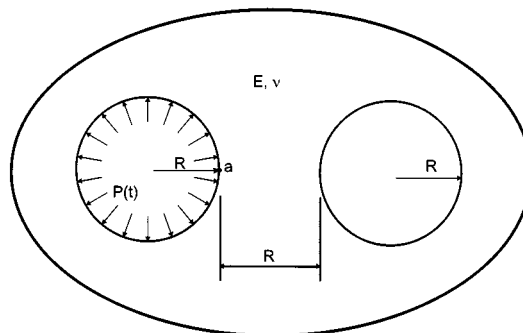


Figure 5. Two cylindrical cavities in an infinite domain

dimensions, since wave effects continue to arrive from all points along the infinitely long out-of-plane integrated direction. An inaccurate accounting for this large time effect in a numerical integration scheme leads to the accumulation of numerical errors as pointed out by Dominguez [2]. Some of the solutions to this problem have included the use of complicated normalization schemes to minimize the accumulation of round-off errors at large times [2], or changing the fundamental solution to converge to the static solution at large times [3, 4].

Similarly, the use of analytical integration may minimize the accumulation of round-off errors at large times, as indicated by the two example problems discussed previously. However, instabilities are observed in the case of more complicated problems, such as the problem shown in Figure 5, consisting of two cylindrical cavities in an infinite domain, with one cavity subjected to a sudden pressurization given by $p(t) = p_0 H(t)$, whereas the other cavity remains unloaded. As in the Selberg problem discussed previously, each cavity is discretized into 16 elements, and the

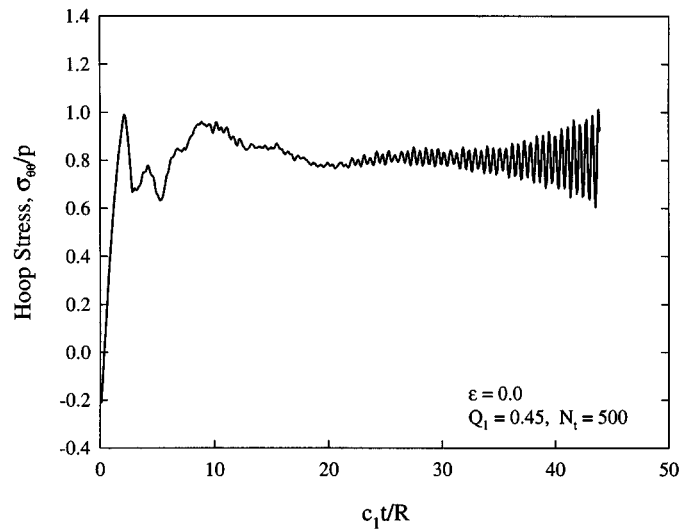


Figure 6. Hoop stresses at point 'a'

shear modulus and Poisson's ratio are the same as for the two previously discussed examples, whereas now $Q_1 = 0.45$, and the number of time steps is $N_t = 500$.

Figure 6 shows the normalized hoop stress at point 'a' (Figure 5). The time history results show clear signs of instability at approximately $c_1 t/R = 20$. To evaluate the effect of different time step sizes on the stability of the two cavities, a series of results were obtained for Q_1 ranging from 0.2 to 1.2, in increments of 0.1. In all cases, instabilities were observed, leading to the conclusion that, even though the use of analytical integration helps the stability of elastodynamic problems significantly, it is insufficient to prevent instabilities for moderately complicated problems, such as the two-cavity problem.

IMPROVED DIRECT BOUNDARY ELEMENT FORMULATIONS

Boundary integral formulations

The time domain elastodynamic boundary integral equations in the time domain can be derived for two-dimensional solids by combining the solution to the governing differential equations of motion (i.e. the fundamental solution of elastodynamics) due to an applied line force with Graffi's [16] dynamic reciprocal theorem. In the absence of body forces, and given zero initial conditions, the resulting integral formulation for a body with a boundary S is as follows:

$$a(\underline{\xi})u_k(\underline{\xi}, t) = \int_S U_{ik}(\underline{x}, t; \underline{\xi}, 0) * t_i(\underline{x}, \tau) ds(\underline{x}) - \int_S T_{ik}(\underline{x}, t; \underline{\xi}, 0) * u_i(\underline{x}, \tau) ds(\underline{x}) \quad (2)$$

where the symbol $*$ denotes the time convolution operator, $U_{ik}(\underline{x}, t; \underline{\xi}; \tau)$ is the k th displacement component at the receiving point \underline{x} at time t due to a unit line load in the i th direction, which was applied at time $t = 0$; and $T_{ik}(\underline{x}, t; \underline{\xi}; \tau)$ is the corresponding k th traction component at the

receiving point \underline{x} , applied at time $t = 0$, and finally $a(\underline{\xi})$ is defined as

$$a(\underline{\xi}) = \begin{cases} 0, & \underline{\xi} \notin V \\ 1, & \underline{\xi} \in V \end{cases} \quad (3)$$

in which V denotes the domain of interest. Both U_{ik} and T_{ik} are given in Eringen and Suhubi [17].

To facilitate the numerical implementation of (2), it is assumed that $\underline{\xi}$ lies outside the domain V , resulting in

$$\int_S U_{ik}(\underline{x}, t; \underline{\xi}, 0) * t_i(\underline{x}, \tau) ds(\underline{x}) = \int_S T_{ik}(\underline{x}, t; \underline{\xi}, 0) * u_i(\underline{x}, \tau) ds(\underline{x}) \quad (4)$$

This formulation allows for the integrals to be evaluated analytically before $\underline{\xi}$ is allowed to approach the boundary, S .

The numerical implementation of (4) requires approximation of boundary field variables in both time and space, by dividing the boundary into N straight-line or curved elements, and the time interval from time 0 to the evaluation time t is divided into m intervals of duration Δt , resulting in

$$\sum_{k=1}^m \sum_{b=1}^N \int_{S_b} U_{ik}^{m-k+1} * t_i^k dS_b = \sum_{k=1}^m \sum_{b=1}^N \int_{S_b} T_{ik}^{m-k+1} * u_i^k dS_b \quad (5)$$

where the loading point $\underline{\xi}$ and the receiving point \underline{x} have been omitted for simplicity, dS_b relates to the spatial integration of the b th boundary element, and t_i^k and u_i^k are the boundary tractions and displacements over the time interval $(k-1)\Delta t$ to $k\Delta t$.

The temporal integrals can be performed analytically [2, 5]. The spatial integrations are often evaluated numerically [2, 3], especially in the case of higher-order geometrical and functional variations over each element. In the case where each element is assumed to be a straight line, these integrals can also be carried out analytically [5].

Temporal and spatial integrations

Because the true temporal and spatial distributions for the tractions and displacements in (4) are not known *a priori*, it is necessary to assume a functional variation in time and space for the boundary tractions and displacements, before the integrals in (5) can be evaluated. The temporal variation within each time step is generally assumed to be either constant or linear. The spatial variation of displacements and tractions over each element is assumed to be constant, linear, quadratic, etc. The displacements and tractions are approximated as

$$u_i(\underline{x}, t^k) = u_i^k \phi(t^k) \theta(S_b) \quad (6)$$

and

$$t_i(\underline{x}, t^k) = t_i^k \phi(t^k) \theta(S_b) \quad (7)$$

where $\phi(t^k)$ and $\theta(S_b)$ are the assumed time and space interpolation functions, u_i^k and t_i^k are the unknown displacements and tractions at discrete time (t^k) and boundary element b . Substituting

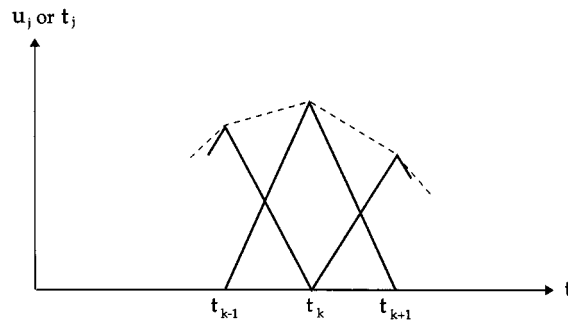


Figure 7. Piecewise linear time variation with triangular hat functions

(6) and (7) into (5) results in

$$\sum_{k=1}^m \sum_{b=1}^N \int_{S_b} \phi(t^k) \theta(S_b) U_{ik}^{m-k+1} t_i^k dS_b = \sum_{k=1}^m \sum_{b=1}^N \int_{S_b} \phi(t^k) \theta(S_b) T_{ik}^{m-k+1} u_i^k dS_b \quad (8)$$

The temporal integrations in (8) can be approximated by various schemes discussed in detail by Peirce and Siebrits [8, 9]. However, the trapezoidal rule is used in most elastodynamic boundary element formulations. In this case we assume a piecewise linear time variation for the boundary displacements and tractions, resulting in $f(t) = H(t)(t/\Delta t)$. The time integrations can then be performed for the special case $u_i(\underline{x}, t^k) (t/\Delta t) u_i^k \theta(S_b)$ and case $t_i(\underline{x}, t^k) = (t/\Delta t) t_i^k \theta(S_b)$. Three of these functions can then be staggered to obtain a ‘hat’ function at each time step, from which the piecewise linear time variation can be constructed. Figure 7 shows the ‘hat’ functions involved in this approach. The combination of the three linear functions of form $H(t)(t/\Delta t)$ results in

$$u_i(\underline{x}, t^k) = \left[H(t - t^{k-1}) \frac{\tau^{k-1}}{\Delta t} - 2H(t - t^k) \frac{t^k}{\Delta t} + H(t - t^{k+1}) \frac{\tau^{k+1}}{\Delta t} \right] u_i^k \theta(S_b) \quad (9)$$

where $t^k = k\Delta t$, and $\tau^k = t - t^k$ and $H(t)$ denotes the heaviside function. A similar equation can also be obtained for the tractions.

The spatial integrations in (8) can be performed either numerically or analytically as discussed by Dominguez [2] and Birgisson and Crouch [5]. The spatial shape functions in (8) can be of any order, such as piecewise constant, linear, or quadratic. However, in higher order formulations the variation in boundary displacements and tractions across the element is typically assumed to be quadratic. In the case of numerical integration schemes the boundary element is often assumed to be curved [2, 3], whereas in analytical integration schemes the boundary elements are assumed to consist of straight-line segments so that the integrals are tractable.

It is very important to account adequately for the sharp spatial variations in displacements and stresses at wavefronts. These variations in boundary parameters are a function of the time history of loading, as well as the causality property of the fundamental solution of elastodynamics, which dictates that a receiver point cannot feel any dynamic effects from a source point before the compressional wave arrives at the receiver point. As discussed previously, an important benefit of using analytical integration is that variable integral limits can be used to ensure that integrations are only performed over the dynamically active parts of each element [5, 15], resulting in solutions that are both causal and highly accurate.

Discretization of boundary integrals

The discretization of (8) is primarily dictated by the type of temporal integration scheme used, as summarized by Peirce and Siebrits [8, 9] for indirect boundary element methods. In the following sections, a similar overview is given for the direct boundary element method. For simplicity, the discussion is restricted to traction boundary value problems, even though the solution procedure can easily be applied to displacement or mixed boundary value problems.

Trapezoidal scheme

The trapezoidal scheme summarized in (9), combined with the discretization of the time and space integrals in (8) leads to a system of time-marching algebraic equations of the form

$$\mathbf{T}_0 \mathbf{u}_m = \sum_{k=0}^m \mathbf{U}_k \mathbf{t}_{m-k} - \sum_{k=1}^m \mathbf{T}_k \mathbf{u}_{m-k} \quad (10)$$

where m represents the current time step number. The terms inside the summation signs represent the time history of the boundary displacements and tractions. The vectors \mathbf{u}_{m-k} and \mathbf{t}_{m-k} represent the nodal displacements and tractions at time $(m-k)\Delta t$, and the matrices \mathbf{T}_k and \mathbf{U}_k are the traction and displacement influence coefficient matrices, respectively, at time $k\Delta t$. In general, the matrices \mathbf{T}_k and \mathbf{U}_k are fully populated. It is clear that the unknown displacements \mathbf{u}_m at the current time step m (when $k=0$) are obtained via a convolution between the known coefficients and known quantities from all previous times in the two-dimensional case. The basis functions for the trapezoidal scheme are shown in Figure 8.

Direct half-step scheme

The so-called direct half-step scheme essentially consists of a two-part time-stepping scheme, where some of the influence coefficients are calculated at a full time step, and alternate ones are calculated at half time steps. The system of equations can be written as

$$\begin{aligned} \mathbf{T}_0^h \mathbf{u}_{2m-1} + \sum_{k=0}^{m-1} \mathbf{T}_{2m-2k-1}^h \mathbf{u}_{2k} &= \sum_{k=0}^{2m-1} \mathbf{U}_{m-k}^h \mathbf{t}_k \\ \mathbf{T}_0^f \mathbf{u}_{2m} + \mathbf{T}_1^f \mathbf{u}_{2m-1} + \sum_{k=0}^{m-1} \mathbf{T}_{2m-2k}^f \mathbf{u}_{2k} &= \sum_{k=0}^{2m} \mathbf{U}_{m-k}^h \mathbf{t}_k \end{aligned} \quad (11)$$

where h implies a half step and f implies a full step. This scheme is a variation of the half-step scheme developed by Peirce and Siebrits [8]. The difference is that the time history traction terms

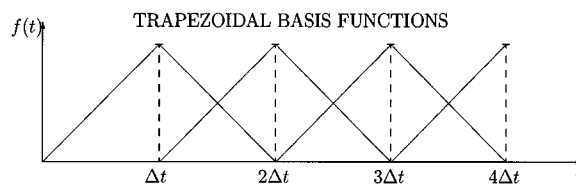


Figure 8. Basis functions for the trapezoidal scheme

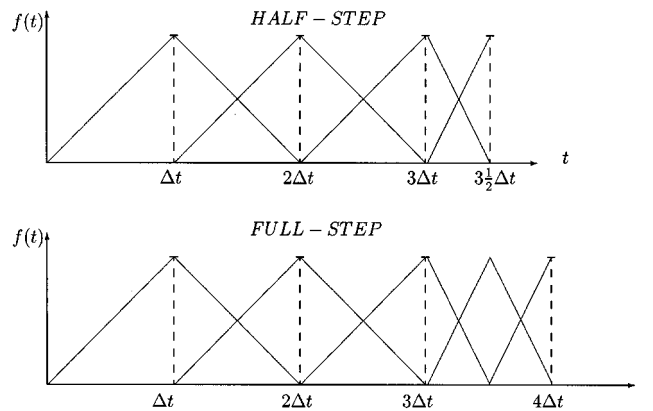


Figure 9. Basis functions for the direct half-step scheme

on the right-hand side of (11) are calculated by the trapezoidal scheme, but are now applied at every half-step, rather than the full time step, as in the original trapezoidal scheme. The basis functions for the direct half-step scheme are shown in Figure 9.

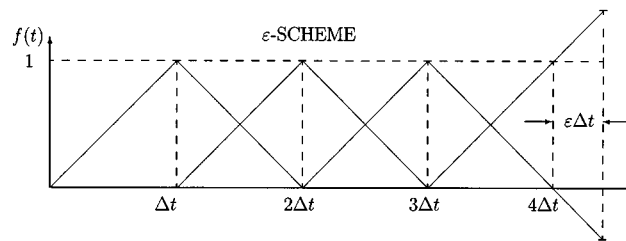
The direct half-step scheme improves the stability properties of the system of equations because it ensures amplified diagonal terms in the influence coefficient matrices while maintaining consistency [8]. However, the scheme only improves the stability properties of the direct boundary element methods for traction boundary value problems. In the case of displacement boundary value problems, the half-step scheme will not improve the stability of the method because of the nature of the influence coefficients as a function of time.

The improved stability characteristics of the half-step scheme for traction boundary value problems can be explained in the following way. The stress and displacement self-effect influence coefficients are of order $O(1)$ and $O(\Delta t)$ in the direct boundary element method. This means that the magnitude of the displacement self-effect influence coefficient is halved if the time step is halved. The stress self-effect is unaffected by the time step. However, it is divided by the displacement self-effect when solving for the unknown tractions, with the resultant effect of doubling the combined self-effect term. This doubling of the leading terms implies that the diagonal entries in the self-effect matrix are doubled in magnitude, which improves the stability properties of the system of the equations.

Epsilon (ε -) scheme

The ε -scheme is a slight variation on the trapezoidal scheme, and trivial to implement. The hat function at the current time step is adjusted by a small amount, $\varepsilon\Delta t$, as shown in Figure 10. The effect of the introduction of this artificial perturbation in the shape function is to increase the magnitude of the diagonal terms in the influence coefficient 'self-effect' matrix. An increase in the magnitude of the diagonal term implies an improvement in the conditioning number of the matrix, which implies improved stability of the system. This has been extensively documented by Peirce and Siebrits [8] for indirect boundary element methods.

In the indirect boundary element methods, this scheme causes an undesirable time shift in the numerical results. However, in the direct boundary element methods, no shift is observed in the

Figure 10. Basis functions for the (ε -) scheme

results as will be seen in Section 4. The displacement and stress influence coefficient matrices tend to cancel out any potential shifts with respect to each other.

STABILITY OF TIME-STEPPING SCHEMES

Illustration of stability characteristics via a test problem

In order to gain some insight into the stability properties of the trapezoidal scheme and the way in which the ε -scheme enhances the stability of the time-stepping process, we consider the following simple demonstration involving the traction influences along the centerline ($x = 0$, $0 \leq y$) due to a horizontal boundary element of width $2a$ located at the origin. We consider the traction influence due to a displacement field u that has the same spatial variation as the quadratic basis function centered on the middle of the sending element and which has been excited by a string of pulses such as those shown in Figures 8 and 10. In Figure 11 we plot the traction influences due to the string of pulses that go to make up the trapezoidal scheme as well as a similar set of pulses for the ε -scheme. All the tractions in this plot have been normalized with respect to the self-effect of the trapezoidal scheme, i.e. the traction influence at the centre of the source element due to a displacement excitation comprising the first quadratic-linear space-time basis function in the trapezoidal sequence.

We observe that the traction influences due to the trapezoidal scheme can be larger at elements that are located away from the sending element. The implication of this is that if a second element were located at the peak $y/2a \approx 0.12$, of the trapezoidal influence curve shown in Figure 11, then a positive feed-back situation can result in which an initial disturbance starting at one of the two elements will be amplified as it is reflected back and forth between the two elements. This will inevitably lead to instability. We observe that the peaks in the trapezoidal influence curve decay as the observation points are moved away from the sending element. We notice that at other than the receiving points in the immediate neighbourhood of the peak $y/2a \approx 0.12$, the subsequent peaks are all lower than the self-effect. Thus one could imagine trying to devise a strategy to stabilize a boundary element discretization in which one limited the spatial separation between any two sending and receiving pairs to be greater than 0.12 element widths. The self-effect in this situation would be larger than the effect on any one of the receiving elements. However, the fact that the self-effect is larger than any one of the remote influences does not guarantee stability either. Indeed, one could imagine a discretization in which a sequence of receiving elements were located at the peaks of the sequence of trapezoidal wave fronts shown in Figure 11. In this case,

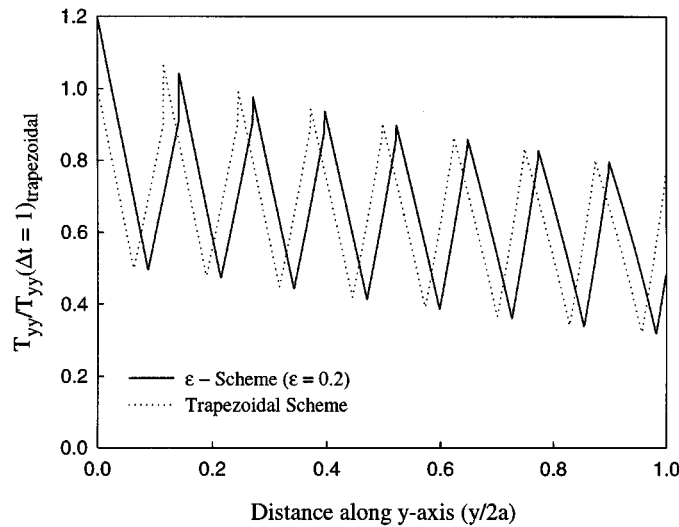


Figure 11. Traction influence curves for the trapezoidal and epsilon (ϵ -) schemes

the total energy reflected back to the sending element by the receiving elements in response to the initial sending element will exceed the energy that was put into the system initially, and an instability would result. We also note from the highly oscillatory nature of the trapezoidal plot (Figure 11) that we can expect that the stability properties of a particular discretization will depend strongly on whether the receiving elements fall in the troughs or close to the peaks of the influence curve of a given sending element. For a given spatial discretization, if we change the time step we can expect the elements to move from troughs to peaks and back again, which explains the sort of intermittent instability properties observed in time domain dynamic boundary element discretizations [8, 9].

The traction influences for the ϵ -scheme have a larger self-effect, while the tractions that a remote receiving element would experience are essentially the same as those that would have been generated by the trapezoidal scheme, but which have been shifted by a distance $\epsilon\Delta t$. As the parameter ϵ is increased, the ϵ -scheme self-effect will be enhanced, while the peaks of the receiving element influence functions will be shifted down the envelope formed by the traction influence functions for the trapezoidal scheme. Thus the stability of any spatial discretization can be substantially enhanced by means of the ϵ -scheme. For the indirect boundary element method, in which the boundary integral equation involves only one integral, the ϵ -scheme discretization of this integral leads to an undesirable shift in the results. For the direct boundary element method, in which the boundary integral equation involves two integrals, the ϵ -scheme discretization of both of these integrals compensates for any possible shift in the solution and no drift in the solution is observed.

Stability analysis

Although the ϵ -scheme is expected to have substantially enhanced stability characteristics, all of the time-stepping methods outlined earlier could possibly be unstable given an unfortunate

combination of spatial and temporal discretizations. Therefore, it is desirable to have a means of analysing a particular discretization in order to be able to tell *a priori* if stability can be guaranteed. For domain discretization methods, such as the finite difference and finite element methods, simple criteria exist based on bounds on the maximum eigenvalues of the discretized spatial operator and the size of the time step. However, the situation for discretized boundary integral equations is quite different as can be seen from the framework for analysing discretized boundary element equations proposed in [8, 9].

In this section we briefly summarize the stability analysis presented in [8] for a model problem comprising the solution of the integral equation

$$u(x, t) = \frac{1}{2c} \int_0^t \int_{x-c(t-\tau)}^{x+c(t-\tau)} f(\xi, \tau) d\xi d\tau \quad (12)$$

which represents the solution to the one-dimensional wave equation

$$\frac{\partial^2 u}{\partial t^2} - c^2 \frac{\partial^2 u}{\partial x^2} = f(x, t) \quad (13)$$

and discuss how the results can be used to predict the stability characteristics of the direct boundary element method.

For simplification, we consider a uniform piecewise constant spatial discretization and trapezoidal and ε -scheme time discretizations of integral equation (12). By means of a spatial Fourier transform and a Z -transform in time, it is possible to determine the rate at which errors will grow or decay for a given discretization, and hence the numerical stability characteristics of the solution [8, 9]. The stability of the constant in space trapezoidal in time discretization of (12) in the case $Q_1 = 1.0$ is determined by the zeros of the so-called transfer function $J(z)$, where the z is the Z -transform variable. We note that, for each value of the spatial Fourier transform variable θ , $J(z)$ has one unstable root at $z \approx -3.732$, one stable root at $z \approx 0.268$, and a complex conjugate pair of roots that are marginally stable so that $J(\theta)$ factors as follows:

$$(z - e^{ia(\theta)})(z - e^{-ia(\theta)})(z + 3.732)(z - 0.268) \quad (14)$$

Thus even for this simple model problem the standard trapezoidal scheme turns out to be unstable. A similar analysis for an implicit scheme in which $1.0 \leq Q_1 \leq 2.0$ shows that as θ varies from π to 0 the zero of $J(z)$ with the larger magnitude changes from being unstable at -3.8 to being stable at -0.2 . Since there are unstable zeros for at least one of the possible values of the parameter θ , the trapezoidal discretization scheme is unstable in spite of the fact that the time stepping scheme is implicit.

Since both the explicit and implicit trapezoidal schemes were unstable, we investigated the ε -scheme to see if it yielded improved stability characteristics for this model problem. We note that the ε -scheme can be regarded as a perturbation to the trapezoidal scheme which reduces to the constant/linear scheme in the special case $\varepsilon = 0$. In the special case $Q_1 = 1.0$, $\varepsilon \leq 0.5$, the transfer function $J_\varepsilon(z)$ for the ε -scheme has a root structure that is similar to that for the trapezoidal scheme in the case $Q_1 = 1.0$. In particular, for small values of ε , the scheme has a single unstable zero. Increasing the parameter ε brings the unstable zero closer to the unit disc, until it finally falls within the unit disc for $\varepsilon \geq 0.4$. For an implicit situation in which $Q_1 = 2.0$, $\varepsilon \leq 0.5$, the zeros of the transfer function $J_\varepsilon(z)$ of the ε -scheme were shown to have a similar

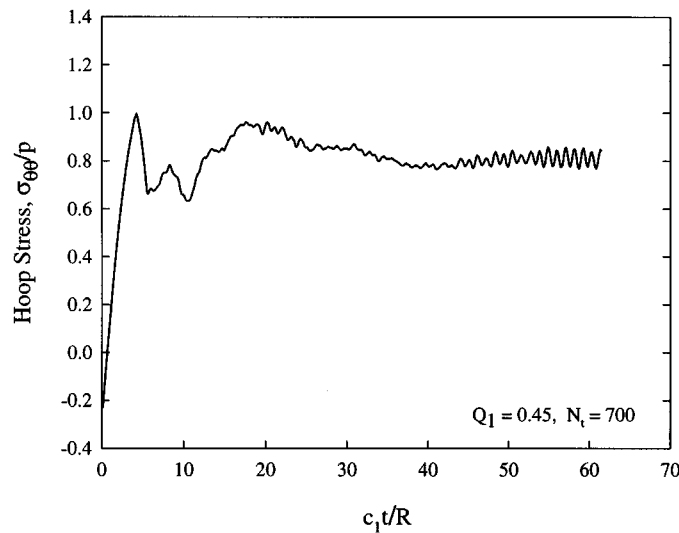


Figure 12. Normalized hoop stress at point 'a'

structure to those for zeros closer to the unit disc until they finally fall within the unit disc for $\varepsilon > 0.366$. Thus the ε -scheme stabilizes the time stepping process as will be seen for the numerical experiments on more general initial boundary value problems presented in the next section.

The analysis presented in [8] clearly illustrates the stabilizing effect of the ε scheme. In order to extend the analysis to more general elastodynamic problems the procedure outlined in [8] should be followed.

PERFORMANCE OF NEW TIME-STEPPING SCHEMES

Direct half-step scheme

To evaluate the effectiveness of the direct half-step scheme, the two cavity problem shown in Figure 5 is revisited. Each cavity is again discretized into 16 elements, and the material properties and loading history of the pressurized cavity are as before, with the exception that the number of time steps is $N_t = 700$.

Figure 12 shows the normalized hoop $\sigma_{\theta\theta}/p$ at point 'a' (Figure 5) versus normalized time $c_1 t/R$. The time history of results shows clear signs of instability beyond normalized time $c_1 t/R = 40$, which is a significant improvement over the results obtained from the trapezoidal scheme (where instabilities were observed beyond $c_1 t/R = 20$), shown in Figure 6 and discussed previously. However, the direct half-step scheme is not sufficient to remove all signs of instabilities for the two-cavity problem.

To evaluate the accuracy of the direct half-step scheme, the first part of the normalized hoop stress time history is plotted in Figure 13 against results obtained with the traditional trapezoidal scheme. The differences between the two time histories are negligible, leading to the conclusion

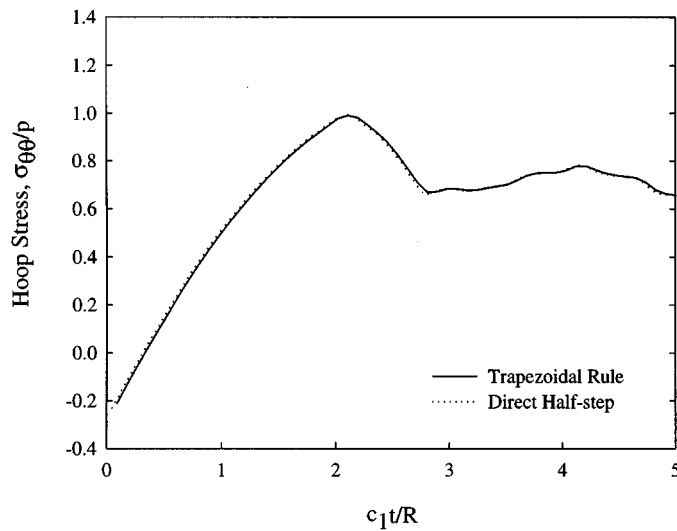


Figure 13. Comparison between the direct half-step and trapezoidal schemes

that the half-step scheme has no adverse effects on the accuracy of the results, and may in fact improve them in some cases as discussed by Siebrits and Peirce [7] and Peirce and Siebrits [8, 9] for indirect boundary element methods.

Epsilon (ε -) scheme

The two-cavity problem shown in Figure 5 is again used to evaluate the effectiveness of the ε -scheme. During the course of this study, the authors found that the problem presented in Figure 5 was an excellent 'check' on the performance of stability schemes for elastodynamic boundary element methods. This problem encapsulates a number of factors that are common in more complicated problems, such as multiple surfaces, intensive reflective wave behaviour, and a severe test of the causality condition in the unloaded portion of the problem. For the evaluation of the ε -scheme, each cavity is discretized into 16 elements, and the material properties and loading history of the pressurized cavity are unchanged, with the exception that the number of time steps is $N_t = 700$, and the value for ε is varied from 0.20 to 0.40. Figures 14(a) and (b) show the results for each ε value in terms of normalized hoop stress $\sigma_{\theta\theta}/p$ at point 'a' (Figure 5) versus normalized time $c_1 t/R$. Figure 14(a) for $\varepsilon = 0.2$ shows clear signs of instability. For $\varepsilon = 0.4$, the instability has disappeared, as shown in Figure 14(b). Note that Figure 14(b) shows results to 2000 time steps. Also, even though the exact value of ε required for achieving stability is problem dependent, as discussed previously, we consistently found that $\varepsilon \geq 0.4$ always resulted in stable results for all problems tested.

To evaluate the effect of different choices of time step on the stability of the case with $\varepsilon = 0.4$, Q_1 was varied between 0.2 and 1.2 in increments of 0.1, for $N_t = 1000$. Figure 15 shows the results for $Q_1 = 1.2$. The rest of the results also showed no signs of instabilities.

Since it is known that the ε -scheme tends to cause a shift in the time history results for indirect time domain boundary element methods [7–9] it is of interest to evaluate the accuracy of the

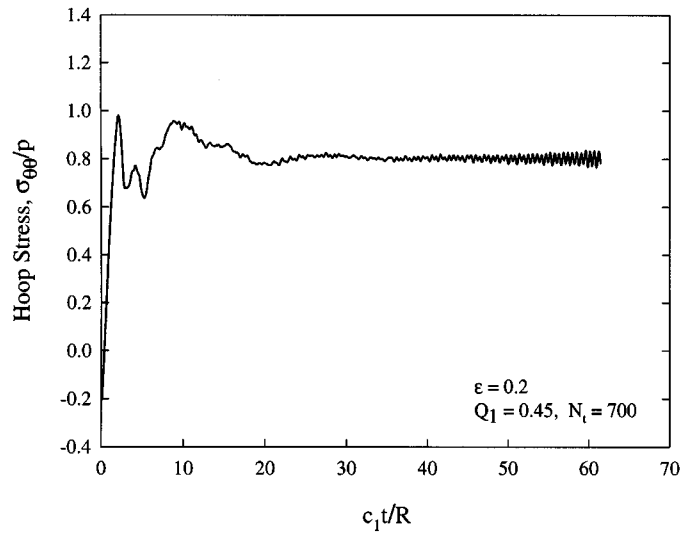


Figure 14(a). Normalized hoop stress at point 'a' for $\varepsilon = 0.2$.

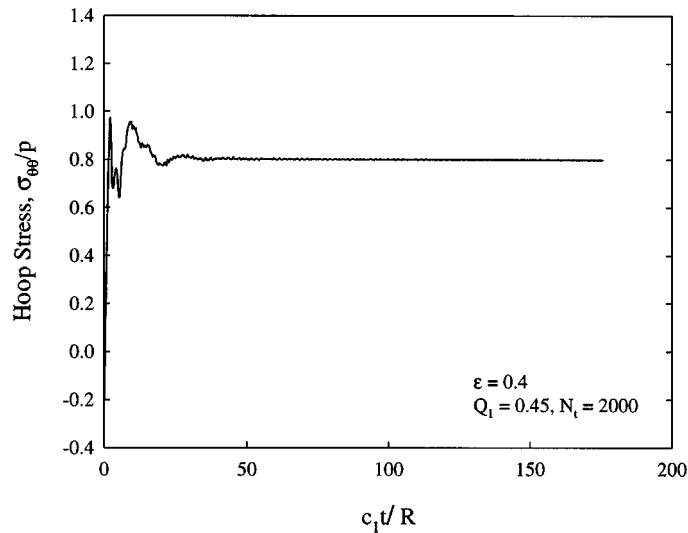


Figure 14(b). Normalized hoop stress at point 'a' for $\varepsilon = 0.4$ and $N_t = 2000$

ε -scheme for a relatively large value of ε , such as $\varepsilon = 0.4$. Figure 16 shows a comparison between the trapezoidal scheme and the ε -scheme for $\varepsilon = 0.4$. The difference in results is negligible. Hence, it can be concluded that the ε -scheme has greatly enhanced stability characteristics, and is as accurate as the traditional trapezoidal scheme.

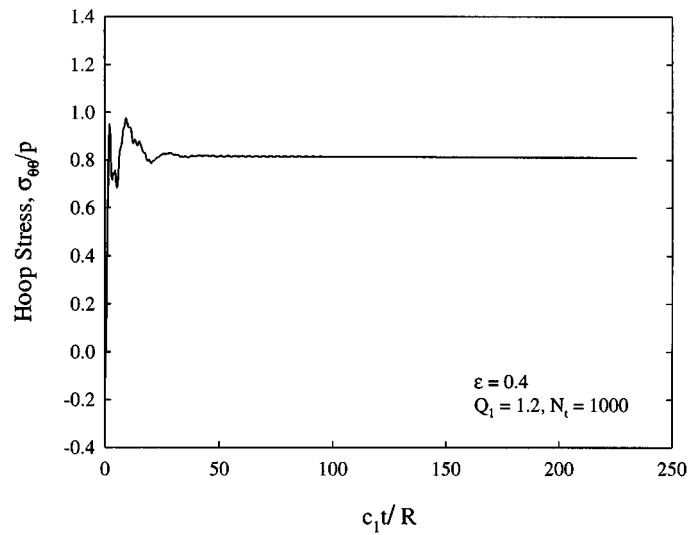


Figure 15. Normalized hoop stress at point 'a' for $\varepsilon = 0.4$ and $Q_1 = 1.2$

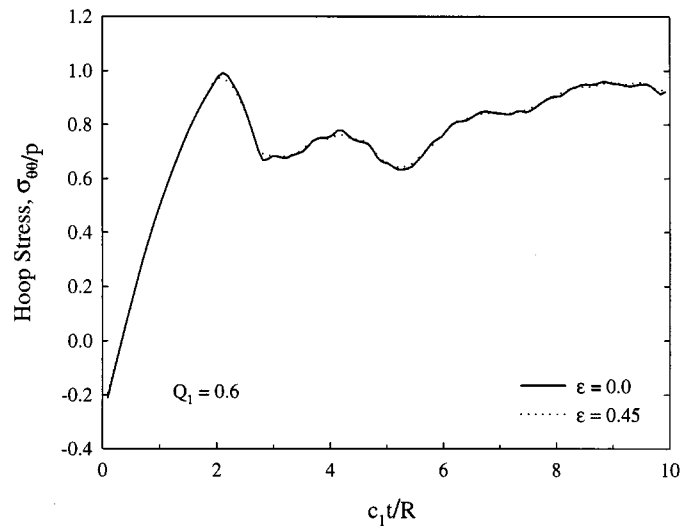


Figure 16. Comparison between the epsilon (ε -) and trapezoidal schemes

CONCLUSIONS

We have shown evidence of numerical instabilities in the direct boundary element method at late times for simple geometric configurations. We have shown that, as the loading or geometric configurations are made more intricate, numerical instabilities are manifested earlier. The results presented in this paper show that higher-order spatial analytical integration schemes tend to

minimize the occurrence of numerical instabilities in the direct boundary element method. We have introduced and demonstrated two new time-stepping algorithms that improve the stability properties of direct boundary element methods. The direct half-step scheme improves the numerical stability of the system but instabilities can still develop at later times. The ε -scheme greatly improves the stability of the direct boundary element method, and, with a sufficiently large choice in the value of ε , no evidence of numerical instabilities is evident, even after a large number of time steps. In addition, this scheme is trivial to implement in any direct boundary element scheme.

REFERENCES

1. Beskos DE. Boundary element methods in dynamic analysis: Part II (1986–1996). *Applied Mechanics Review* 1997; **50**:149–197.
2. Dominguez J. *Boundary Elements in Dynamics*. Computational Mechanics Publications: Southampton, 1993.
3. Israil ASM, Banerjee PK. Advanced time-domain formulation of BEM for two-dimensional transient elastodynamics. *International Journal for Numerical Methods in Engineering* 1990; **29**:1421–1440.
4. Israil ASM, Banerjee PK. Two-dimensional transient wave propagation problems by time-domain BEM. *International Journal of Solids and Structures* 1990; **26**:851–864.
5. Birgisson B, Crouch SL. Elastodynamic boundary element method piecewise homogeneous media. *International Journal for Numerical Methods in Engineering* 1998; **42**:1045–1069.
6. Siebrits E, Birgisson B, Peirce AP, Crouch SL. On the numerical stability of time domain boundary element methods. *International Journal for Blasting and Fragmentation* 1997; **1**(3):305–316.
7. Siebrits E, Peirce AP. Stability properties of time domain elastodynamic boundary element methods. In *Boundary Element Methods*, vol. 17. Brebbia CA (ed.). Computational Mechanics Publications: Southampton, 1995.
8. Peirce A, Siebrits E. Stability analysis of model problems for elastodynamic boundary element discretizations. *Numerical Methods for Partial Differential Equations* 1996; **12**:585–613.
9. Peirce A, Siebrits E. Stability analysis and design of time-stepping schemes for general elastodynamic boundary element models. *International Journal for Numerical Methods in Engineering* 1997; **40**:319–342.
10. Fukui T. Time marching analysis of boundary integral equations in two dimensional elastodynamics. In *Innovative Numerical Methods in Engineering*, Shaw RP *et al.* (eds). Springer: New York, 1986; 405–410.
11. Tian Y. A two-dimensional direct boundary integral method for elastodynamics. *Ph.D. Thesis*, University of Minnesota, USA, 1990.
12. Mansur WJ. A time-stepping technique to solve wave propagation problems using the boundary element method. *Ph.D. Thesis*, Southampton University, UK, 1983.
13. Antes H. A boundary element procedure for transient wave propagation in two-dimensional isotropic elastic media. *Finite Element Analysis and Design* 1985; **1**:313–322.
14. Manolis GD, Ahmad S, Banerjee PK. Boundary element method implementation for three-dimensional transient elastodynamics. In *Developments in Boundary Element Methods-4*, Banerjee PK, Wilson RB (eds). Elsevier: New York, 1986; 29–65.
15. Siebrits E, Crouch SL. Two-dimensional elastodynamic displacement discontinuity method. *International Journal for Numerical Methods in Engineering* 1994; **37**:3229–3250.
16. Graffi D. Sul teorema di reciprocita nella dinamica dei corpi elastici. *Memoria della Accademia della Scienze, Bologna Ser 10* 1947; **4**:103–111.
17. Eringen AC, Suhubi ES. *Elastodynamics*. Academic Press: New York, 1975.